Available online at www.sciencedirect.com

ScienceDirect

journal homepage: www.elsevier.com/locate/he

# Influence of the operation mode on PEM water electrolysis degradation

*Steffen Henrik Frensch* [a,*], *Frédéric Fouda-Onana* [b], *Guillaume Serre* [b], *Dominique Thoby* [b], *Samuel Simon Araya* [a], *Søren Knudsen Kær* [a]

[a] *Aalborg University, Department of Energy Technology, Pontoppidanstræde 111, 9220, Aalborg Øst, Denmark*
[b] *CEA, LITEN, DEHT, F-38054, Grenoble, France*

## HIGHLIGHTS

- Dynamic operation does not enhance degradation.
- Effect of membrane thinning was separated from other degradation mechanisms.
- Temperatures above 80 °C require mitigation strategies for all components.

## GRAPHICAL ABSTRACT

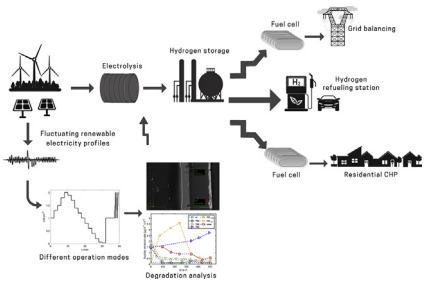


## ARTICLE INFO

*Article history:*
Received 6 December 2018
Received in revised form
19 September 2019
Accepted 21 September 2019
Available online xxx

*Keywords:*
Polymer electrolyte membrane
Water electrolysis
Membrane degradation
Dynamic operation mode
Durability

## ABSTRACT

This paper compares the performance over time of seven different operation modes with the scope of investigating realistic degradation responses of a polymer electrolyte membrane water electrolysis (PEM WE) to different operation modes for grid-balancing services. Among these modes are constant current and constant voltage operations at different temperatures and current cycling operations, including a solar profile. It was found that faster current cycling improved the overall cell performance over the test period of 500 h, mainly due to a decrease in total ohmic resistance, which is also observed during the break-in phase preceding the experiments. Dynamic operation led to more severe fluoride emission from the catalyst binder, which improved the performance in terms of cell potential but could be a concern for long term degradation as membrane thinning promotes higher gas crossover. All other operation modes on the other hand suffered from an increase in total ohmic resistance, leading to an overall performance decrease, which is suspected to be due to the passivation of the Ti components. Higher operating temperatures were found to enhance cell performance, but are detrimental from a durability point of view since they exacerbate both membrane thinning and passivation processes.



* *Corresponding author.*
E-mail addresses: sfr@blue.world (S.H. Frensch), frederic.fouda-onana@cea.fr (F. Fouda-Onana), guillaume.serre@cea.fr (G. Serre), dominique.thoby@cea.fr (D. Thoby), ssa@et.aau.dk (S.S. Araya), skk@et.aau.dk (S.K. Kær).
https://doi.org/10.1016/j.ijhydene.2019.09.169

## Introduction

Hydrogen may play an important role in future energy systems, where transition from fossil fuels to fluctuating renewable energy sources such as solar and wind will require large-scale energy storage solutions. In this context, hydrogen production through polymer electrolyte membrane water electrolysis (PEM WE) is gaining increasing attention [1,2]. The technology may be utilized for energy storage by producing hydrogen for a later use to convert it back into electrical energy or thermal energy. Besides using gaseous hydrogen directly in fuel cells (FC), it can also be part of power-to-x systems, including the production of syngas or liquid fuels such as methanol [3–5]. Furthermore, due to their fast response times, PEM electrolyzers may take over grid services such as frequency stabilization [1,6,7], which are now mainly provided by conventional thermal turbines through their inertia. Last but not least, water electrolysis presents a potentially $CO_2$ neutral alternative to natural gas reforming for industrial hydrogen production.

Although the PEM technology for both fuel cells and electrolysis is well researched, a wide market implementation is not yet observed. One of the biggest challenges is the high cost of production, which has to be addressed both by lowering material cost and by extending the useful lifetime of the system. An increasing amount of literature is available on the topic, but especially degradation under dynamic operation calls for more research. The most comprehensive work with the focus on dynamic operation can be found in Ref. [8], where the authors compare different operation modes in terms of degradation rates. The work comes to the conclusion that cycling operation may be beneficial in terms of hydrogen-output-normalized degradation rates. It is based on their previous work, where the major degradation cause in constant operation was identified as passivation of the porous transport layer (PTL) made of titanium due to oxidation [9]. Ti-PTL passivation together with membrane thinning was also found by other authors [10].

Degradation is also observed under constant operation in the anode catalyst layer (CL) [11], and within the ionomer (membrane and catalyst layer) due to impurities from the feed water, which increase ionic and charge transfer resistance [12]. Fluoride emission has long been utilized in PEM fuel cell degradation studies as an indicator for membrane degradation [13,14]. Since PEM WE often uses the same Nafion®- based membrane, which only differs in thickness, the method can also be applied for electrolysis [10]. Fluoride in the effluent water must originate from the Nafion® ionomer either in the membrane or the catalyst layers, and can be correlated to the membrane degradation [10,15].

This work provides a systematic study of the effect of different dynamic operation modes on PEM WE degradation. Different load cycling operation modes as well as direct coupling to a photovoltaic system were investigated to simulate PEM WE participation in the grid. Furthermore, the effect of elevated temperature is investigated, as operation above 80 °C is desirable in terms of efficiency and commercialization [16].

## Methodology

### *Experimental setup*

All experiments were carried out on a single cell test set-up. The catalyst inks and membrane-electrode-assemblies (MEAs) with an active area of 25cm$^2$ were produced in house, with an ink composition of 34.7wt-% $H_2O$, 5wt-% $IrO_2$, 49.5wt-% isopropyl alcohol, and 10.9wt-% Nafion® D520 dispersion. The circular electrodes were sprayed on Teflon® sheets and transferred onto a Nafion® 115 (N115) membrane through hot-pressing. The transfer was done at 170 °C for 5 min at 300 kg followed by 2 min at 2000 kg. The MEA for a high temperature experiment is an exception, where Nafion® 117 (N117) was used to avoid gas crossover rates at dangerous levels. The cathode, where the hydrogen evolution reaction (HER) takes place, is based on 1.0mgcm$^{-2}$ carbon-supported platinum (Tanaka TEC10V50E), the anode for the oxygen evolution reaction (OER) consists of 2.3mgcm$^{-2}$ iridium-oxide (Surepure Chemetals). Commercial SGL Sigracet® 28BCE carbon sheet and a 1 mm titanium sinter (Accumet, 30% porosity) act as the porous transport layer (PTL) on the cathode and anode, respectively. Both flow fields with parallel channels were made of titanium.

An external power supply was used to monitor current and voltage during the tests. All electrochemical characterizations were carried out with a Biologic HCP-803 potentiostat, which replaced the external power supply during each characterization phase. The setup used in this work is illustrated in Fig. 1.

### *Procedures*

All cells were subjected to the same break-in phase prior to testing. The procedure includes current steps at lower and higher frequencies, and periods of constant current, where one cycle lasts around 40 min and is repeated for around 60 h.

The cell characterization included recording the polarization curve (IV-curve), the anode-side cyclic voltammogram (CV), electrochemical impedance spectroscopy (EIS) measurements at several currents, and collecting an effluent water sample at both anode and cathode for fluoride analysis. Polarization curves were measured in ascending direction in flexible steps from 0.01 to 2.0Acm$^{-2}$ to capture the low current range, which is dominated by activation losses, sufficiently well. This was then followed by galvanostatic EIS measurements at 0.1, 0.5, 1.0, 1.5, and 2.0Acm$^{-2}$. The frequency range was set to 60000 Hz–0.1 Hz, with 10 points per decade and an AC amplitude of 5% of the value of the DC operation point. For this work, the impedance data is used to extract the intercepts with the x-axis in the Nyquist representation at high and low frequency. The high frequency intercept (HFR) represents all ohmic resistances of the cell assembly, whereas the low frequency intercept (LFR) represents the overall polarization resistance.

During the CV measurements, the cathode side was flushed with hydrogen gas, while the DI water flow rate on the anode side was kept constant. Measurements with scan rates of 300 and 50 mV s$^{-1}$were recorded. Furthermore, a sample of

Please cite this article as: Frensch SH et al., Influence of the operation mode on PEM water electrolysis degradation, International Journal of Hydrogen Energy, https://doi.org/10.1016/j.ijhydene.2019.09.169

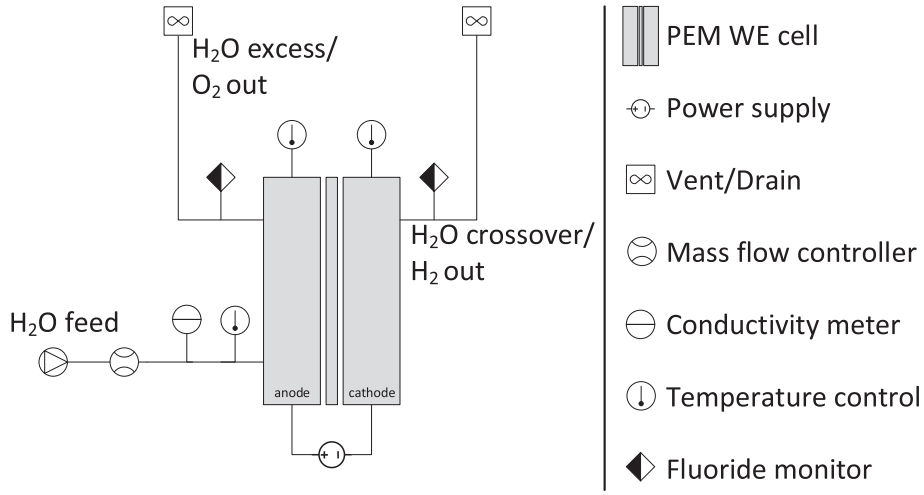


**Fig. 1 – Test set-up for all experiments. The power supply was replaced by a high current potentiostat during characterization.**

effluent water at anode and cathode outlets at 0.3Acm$^{-2}$ was collected for each test point. As a trade-off between the need for capturing steady state ion concentrations and short collection time to exclude capturing transients, the effluent water was collected for 150 s at the anode and 1 h at the cathode side. The samples were then analyzed in an ion chromatograph (Thermo Scientific DIONEX® ICS 2100) for fluoride content.

The tests were performed at atmospheric pressure with a constant feed water flow rate of 500 mL h$^{-1}$without recirculation. The feed water was preheated to the operating temperature and its conductivity was monitored throughout the whole test to ensure sufficient quality of 18.2 MΩ• cm. Additionally, heater pads were installed on both sides of the cell for a homogeneous temperature distribution within the cell.

Each experiment was run for at least 500 h. Table 1 summarizes the investigated operation modes. The parameter of interest besides temperature was the current profile. Therefore, one constant and three dynamic current profiles were tested. The solar profile was constructed from data of a real solar photovoltaic system over 16 h, where the mean value was around 1.0Acm$^{-2}$ and the dwell time of 60 s. The periods of the two current cycling profiles, 100 s and 10 s, were extracted by a Fourier transformation of the solar profile. Although no clear dominant frequency was identified, two broad peaks were observed at the highest frequencies, and were chosen as the dwell times for the dynamic operation modes.

Finally, an ex-situ post-mortem analysis was done on the MEAs using a ZEIS LEO 1530 scanning electron microscope (SEM). All samples were taken from the same spot in the middle of the MEA, put into a resin and polished for examination.

**Table 1 – Investigated operation modes. Each experiment was carried out on a fresh cell assembly after a break-in of at least 500 h. All cycling tests were performed at 80 °C.**

| Operation mode (name) | Test condition |
|---|---|
| constant current at 80 (*cc*) | 2.0Acm$^{-2}$ |
| constant voltage at 60 (*T60*) | 2.0 V |
| constant voltage at 80 (*T80*) | 2.0 V |
| constant voltage at 90 (*T90*) | 2.0 V |
| 100 s current cycling ($cyc_{100s}$) | 0–2.0Acm$^{-2}$, 100 s dwell time |
| 10 s current cycling ($cyc_{10s}$) | 0–2.0Acm$^{-2}$, 10 s dwell time |
| Solar PV profile (*Solar*) | 0–2.0Acm$^{-2}$, 60 s dwell time |

## Results and discussion

This section presents the discussion on the comparative analysis of the different operation modes investigated in this paper. Since the current work aims at better understanding dynamic operation modes for grid servicing, more focus is given to the analysis of the fastest current cycling experiment, between 0 and 2.0Acm$^{-2}$ with dwell time of 10 s at each current density at 80 °C. Hereafter, the operation modes are compared among each other.

### *Cell voltage degradation rates*

Fig. 2 shows the voltage degradation rate at 0.1, 0.5, 1.0, and 2.0Acm$^{-2}$ relative to the beginning of life value. That is, the last point represents the rate for the period between 0 h and 506 h, which illustrates the overall impact until the end of the experiment. Since the parameter represents a voltage change, positive values indicate a loss in performance (voltage increase), whereas negative values indicate a gain in performance (voltage decrease).

When looking at the entire duration of the experiment in Fig. 2, it can be seen that the performance at 2.0Acm$^{-2}$ after 500 h is better than at the beginning of life. However, when looking at the evolution of the voltage degradation rate at 2.0Acm$^{-2}$, the degradation rate increases from around −250 μV h$^{-1}$during the first period to around 75 μV h$^{-1}$during the last period of operation. This means that the performance at higher current density increases first before a performance decrease can be observed at the 338 h mark. This is not the

Please cite this article as: Frensch SH et al., Influence of the operation mode on PEM water electrolysis degradation, International Journal of Hydrogen Energy, https://doi.org/10.1016/j.ijhydene.2019.09.169

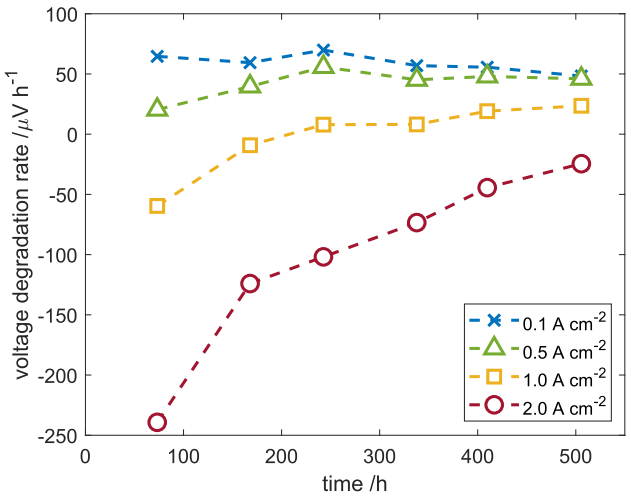


**Fig. 2 – Voltage degradation rates at different current densities relative to the beginning of life (after break-in). Positive values indicate performance decrease, while negative values indicate a performance increase.**

case for low current density operation (0.1 and 0.5Acm$^{-2}$), which is dominated by activation losses, where the degradation rates are positive throughout the duration of the experiment and are relatively constant around 50 μV h$^{-1}$over time. This behavior suggests that the initial increase in performance is of ohmic or mass transport nature, since these processes are more pronounced at higher current densities.

The mean voltage degradation rates over the entire duration of the test for each operation mode are shown in Fig. 3. The graph reveals that fast cycling and the solar profile are the only modes with a negative value (−25.0 and −19.0 μV h$^{-1}$). According to the results, a temperature increase from 60 °C to 80 °C has a moderate negative impact on the degradation rate, from 1.2 to 3.0 μV h$^{-1}$, while operating at 90 °C was found to be significantly more detrimental at 183.8 μV h$^{-1}$. The results ultimately show that the degradation rate decreases with cycling rate and increases with temperature. Moreover, the

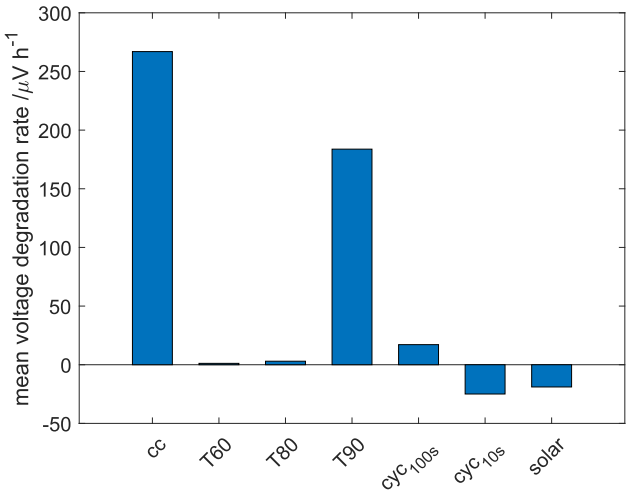


**Fig. 3 – Mean voltage degradation rates at 2.0Acm$^{-2}$ after each experiment was terminated.**

experiment at constant current (cc) exhibits a much higher voltage degradation than the other experiments at 80 °C. Even though, constant operation at 2.0Acm$^{-2}$ has been reported to negatively affect durability compared to other operation modes [9], the here observed high rate is suspected to at least partly stem from the slightly different cell design of that experiment, where a thin gold foil was inserted into the cell assembly in an attempt to monitor contact resistances. This slight modification may have affected the pressure distribution or cell tightness, thereby leading to a higher degradation rate.

Voltage degradation rates per mole of hydrogen produced have also been calculated. The averaged values for the experiments *cc*, $cyc_{100s}$, $cyc_{10s}$, and *solar*are 286.1, 36.7, −53.5, and −40.8μV/$mol_{H_2}$, respectively. It should be noted that the calculations were done on a theoretical basis according to Faraday's law of electrolysis, where potential losses such as gas crossover are neglected. These values can be more useful in further cost analyses, for instance, when the operating and capital costs are to be compared to the revenue. Potential revenue streams besides the obvious monetization of the produced hydrogen include offering grid services as described in the introduction. In such cases, molar-based degradation rates may be more relevant than time-based degradation rates, since the hydrogen production changes with current. Therefore, the cost of energy per unit of produced hydrogen will vary based on the operating conditions and the state of health of the electrolyzer.

### *Catalyst layer degradation*

Qualitatively, the SEM images reveal that the cathode catalyst layer is relatively thick with around 20 textmum due to the carbon-support, and does not exhibit severe damage as seen in Fig. 6. It can also be observed that the catalyst layer and the membrane adapted to local variations, especially on the anode side.

The evolution of the anodic electrode charge as extracted from the CV is shown in Fig. 4. The charge was normalized by area and calculated from the integral of the forward scan between 0.4 V and 1.2 V divided by the geometric area of 25 cm$^2$. There is no visible degradation in the evolution of charge, which may be explained by the high anode catalyst loading that supposedly benefits CL durability [17]. In fact, the measured charge increased by around 10%, which has been observed in other studies in the literature as well [18]. This can be connected to an adjustment of the structure of the catalyst layer to local inhomogeneities in the first period of operation, which has been reported to affect the contact resistance [9], but is here suspected to also have a positive effect on available active sites. Therefore, it can be concluded that the anode catalyst layer is not responsible for a major voltage change. This is further described in Evolution of resistances, where the evolution of the resistances is analyzed.

### *Membrane and ionomer degradation*

Perfluorinated membranes such as Nafion® are known to potentially experience fluoride loss over time. In this work, Nafion® is used for the membrane as well as the binder within

Please cite this article as: Frensch SH et al., Influence of the operation mode on PEM water electrolysis degradation, International Journal of Hydrogen Energy, https://doi.org/10.1016/j.ijhydene.2019.09.169

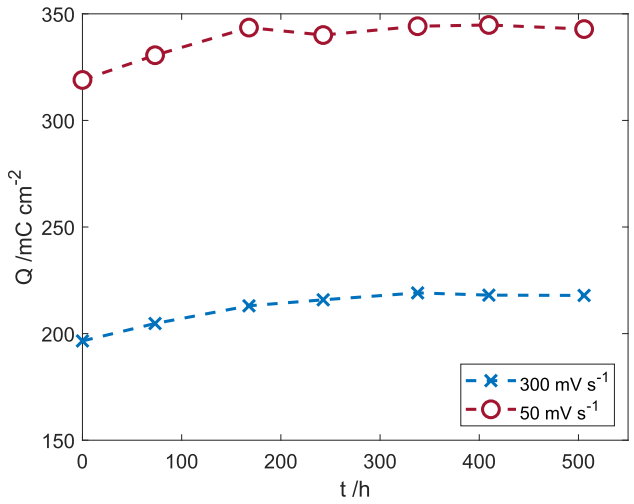


**Fig. 4 – Evolution of anodic electrode charge extracted from CV at 50mV s$^{-1}$ and 300mV s$^{-1}$ over time for experiment.cyc$_{10s}$**

the CL, making both components prone to degradation. The fluoride emission rate was measured through its concentration in the effluent water as shown in Fig. 5 for the fast current cycling experiment, cyc$_{10s}$.

It can be seen that the fluoride emission at the anode outlet is generally lower compared to the cathode outlet at the same operation point, with the exception of the beginning of life, where the emission from the cathode side is almost non-existent. While the fluoride emission rate remains somewhat constant on the anode side at around 0.18 μg h$^{-1}$cm$^{-2}$, it varies significantly on the cathode side. Even though, the cause of the big changes in fluoride emission rates on the cathode side is not clear, it can be said that the ionomer degradation is more severe on the cathode side of the cell. This has been observed in the literature [10] and is true for all operation modes in this work.

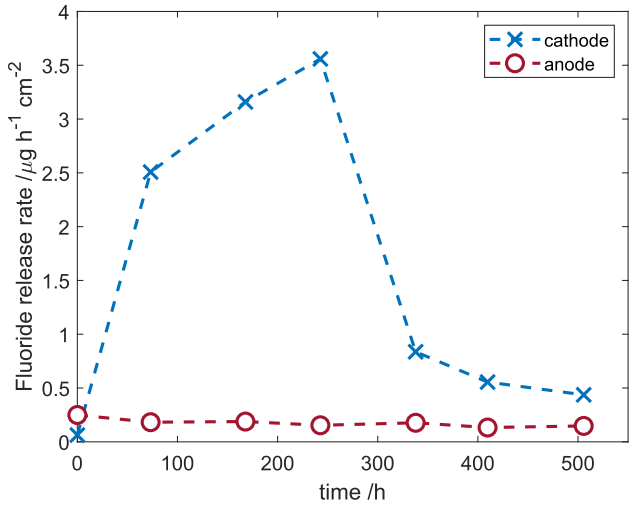


**Fig. 5 – Evolution of fluoride emission rates over time normalized to area at the anode and cathode outlets for experiment.cyc$_{10s}$**

Based on these results and literature survey, the following may be a plausible explanation of the observed degradation mechanism. Oxygen produced at the anode may cross the membrane and react with hydrogen to produce hydrogen peroxide in the presence of the cathodic platinum catalyst [19]. Subsequently, metallic ions from impurities within the PEM WE system may catalyze hydroxyl radical ($HO^{\cdot}$)formation from hydrogen peroxide via the Fenton reaction, which has been suggested for PEM FC [15]. The radicals in turn attack the ionomer, leading to detectable fluoride emission [20]. In the current work the fluoride originates from both the membrane and ionomer binder, since they both contain Nafion® which makes it difficult to directly correlate the fluoride emission with membrane thinning.

To investigate the structural changes and membrane thinning, which among other things can result from the above discussed fluoride loss [21], SEM image comparison of used MEA and fresh membrane was used as shown in Fig. 6a. The image of the MEA after being used in the fast cycling experiment (cyc$_{10s}$) is shown in Fig. 6b, where a thinning effect was observed. The difference in thickness was 17 μm, which corresponds to a thinning rate of 33.7nm h$^{-1}$. However, some parameters, such us water uptake and cell compression can influence the extraction of quantitative data from SEM images [22]. To minimize these effects all the experiments were carried out at the same cell compression levels and all the MEAs were subjected to the same procedures for post-mortem analysis after the cell disassembly. Moreover, all the samples were taken from the middle of the MEA to ensure the highest possible comparability, and were approximately 1 cm × 0.5 cm in size.

As discussed above, the fluoride emission at the cathode is higher. Therefore, Fig. 6b shows only the values at the cathode outlet over time for all operation modes. Even though, no clear trend with regard to the time can be extracted, most of the operation modes exhibit the highest emission rate at the beginning of the test followed by a decline. While the fluoride release rates for the contant current test, cc remain unaltered during the entire test period, the rates at high temperature operation, T90 increase continuously. Even though, the sudden increase and drop in the emission rates for the 10 s current cycling operation can be an experimental error, there is a general decreasing trend towards similar final $F^{-}$emission rates at the final stages of all the operation modes except for operation at 90 °C, where the continuous increase in not arrested within the duration of the test. This could be due to the fact that there is significant contribution from the ionomer binder to the fluoride release rate in the initial phase, which exhausts at the final stages of the tests. Finally, it can be said that fluoride release rates increase with temperature, and the continuous significant increase in fluoride loss rates at 90 °C may indicate that high operating temperatures severely degrade the membrane and should be avoided.

The values of the fluoride mass release for the entire test period of each operation mode, calculated as the integral of each curve can be seen in Fig. 7b. It can be seen, that an increase in temperature leads to an increase in fluoride emission. The change from 60 °C to 90 °C is accompanied by an increase in fluoride emission by one order of magnitude from 1.8 mg to 27.0 mg. The total fluoride emission at 80 °C is 5.4 mg,

Please cite this article as: Frensch SH et al., Influence of the operation mode on PEM water electrolysis degradation, International Journal of Hydrogen Energy, https://doi.org/10.1016/j.ijhydene.2019.09.169

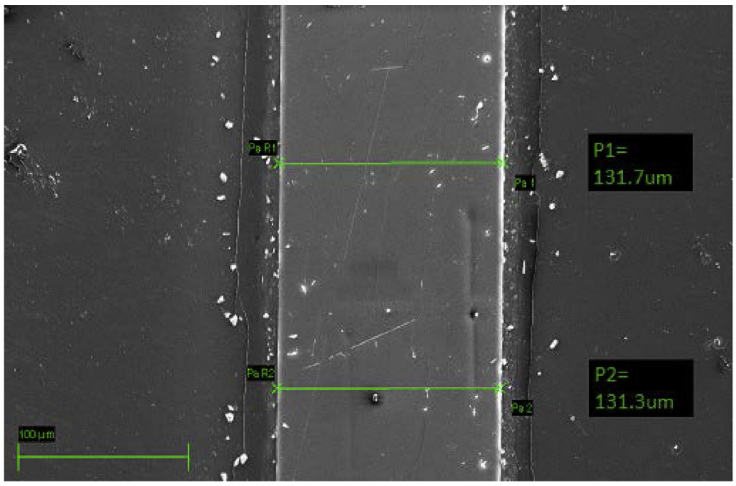


(a) Fresh Nafion®-115 membrane without catalyst layers

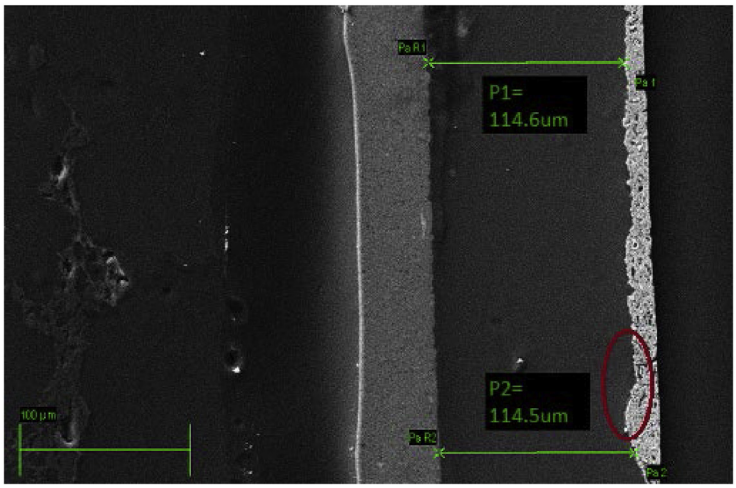


(b) MEA including cathode PTL after experiment $cyc_{10s}$. The cathode is on the left, the anode on the right. The circle indicates an example of adjustments to local variations

**Fig. 6 – SEM images before and after experiment $cyc_{10s}$ to extract qualitative and quantitative data.**

suggesting a non-linear relationship with temperature. Cycling at 100 s dwell time, which was also carried out at 80 °C, leads to a similar value of 4.0 mg. However, the two more dynamic experiments $cyc_{10s}$ and *solar*exhibit an elevated emission of 22.8 mg and 11.2 mg, respectively. Since they are also operated at 80 °C, it can be concluded that dynamic operation leads to higher fluoride emission.

Therefore, even though it appears that dynamic operation has advantages in terms of voltage degradation rates as shown in Fig. 3, this may be at cost of structural damage to the MEA as indicated by the higher fluoride release rates with increasing current cycling rates in Fig. 7. However, longer test periods with non-Nafion® -based ionomers are required to investigate whether faster current cycling also exacerbates membrane degradation or the observed phenomenon only refers to the ionomer binder in the first few hundred hours.

As SEM microscopy is destructive and therefore only carried out at the end of each experiment, a membrane thickness tracking over time is not possible. However, Fig. 7b summarizes the thinning after each experiment measured through SEM except for the *solar*profile, as it was not terminated at the time of writing. Since all the other experiments were carried out for 500±5 h, the values are comparable. The extracted thickness loss for the three temperature-experiments is coherent with their respective fluoride loss, where the test at 90 °C led to almost 35% decrease. It should be noted, that this experiment utilized a N117 membrane, which is considered the same as N115 in terms of chemical structure except for the thickness. The influence of dynamic operation on the other hand is somewhat contradictory to the fluoride emission. Experiment $cyc_{100s}$exhibits an increase in thickness, while experiment $cyc_{10s}$has less decrease than experiment T80, which is not what would be expected from the fluoride emission data. The increase in thickness may not be explained physically. A higher water uptake compared to the fresh N115 sample may explain the difference [22], or coincidentally taking the sample from a portion of the membrane, where it was locally thicker from the beginning. However, it is possible that the operation mode shifts the major point of attack from the membrane to the ionomer content in the CL. This may explain a high fluoride emission without evidence of

Please cite this article as: Frensch SH et al., Influence of the operation mode on PEM water electrolysis degradation, International Journal of Hydrogen Energy, https://doi.org/10.1016/j.ijhydene.2019.09.169

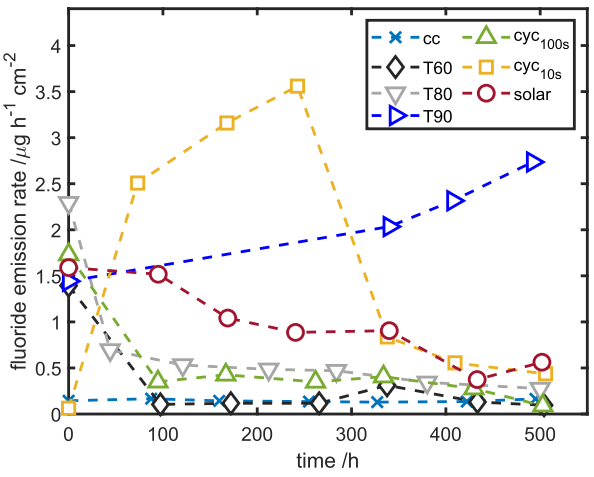


(a) Fluoride emission rates at the cathode outlet over time

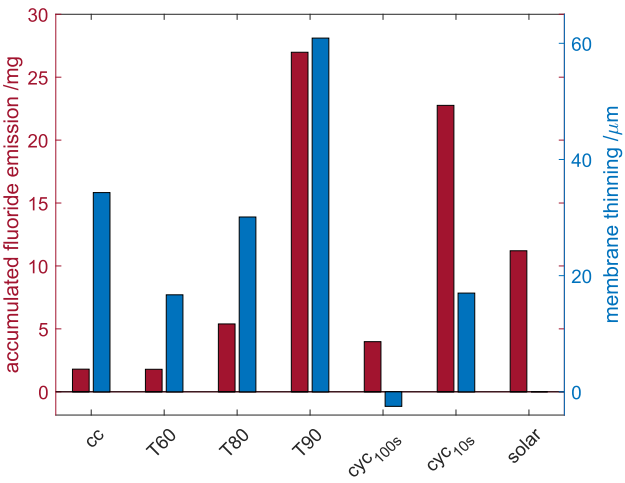


(b) Accumulated fluoride emission and membrane thinning after each experiment as extracted from SEM images

**Fig. 7 – Comparison of fluoride emission (all experiments) and membrane thinning (all experiments except *solar*).**

accelerated membrane thinning. To follow on this hypothesis, the impedance data is further analyzed.

### *Evolution of resistances*

The LFR represents the polarization resistance and should therefore be equal to the slope of the IV curve at the specific operation point. Fig. 8 shows both values at 2.0Acm$^{-2}$ over time together with the HFR (left y-axis), and the difference between LFR and HFR (right y-axis) for experiment $cyc_{10s}$.

The values of LFR and IV slope do correlate quite well, which is seen as a proof of the integrity of the recorded data. Therefore, from now on only the LFR is used to quantify the polarization resistance of the cell. It can be seen that the HFR as well as the LFR are decreasing within the first 338 h, before both show a slight increase for the rest of the experiment.

To see if the increase in performance solely stems from the decrease in HFR, the difference between LFR (equivalent to the polarization resistance) and HFR (total ohmic resistance) is calculated. If this was the case, the difference would be

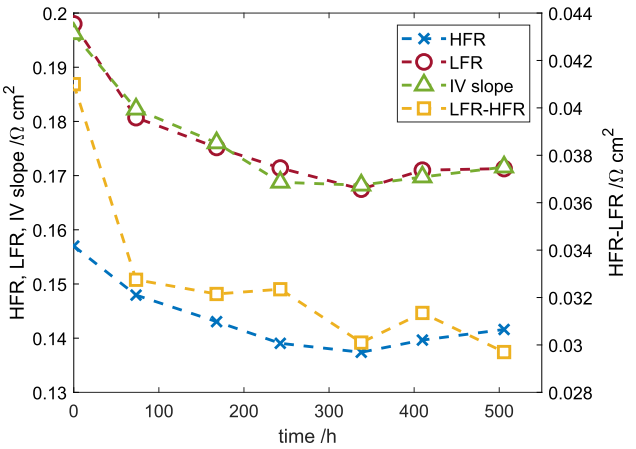


**Fig. 8 – Evolution of resistances over time for experiment $cyc_{10s}$. HFR, LFR (left axis), and their difference (right axis) were extracted from EIS measurements at 2.0Acm$^{-2}$, IV slopes (left axis) from polarization curves.**

constant. However, the values are shown in Fig. 8 and reveal a decrease in difference over time. This suggests that there is also another component involved in the performance gain, where the major share of around 8 mΩcm$^2$is attributed to the first ~ 100h of operation. Afterwards, the value stabilizes and further decrease is negligible with around 2mΩcm$^2$ during a period of 400 h of operation. The initial drop correlates well with the observed increase in charge within the first ~ 150h and may be connected to an improved mass transport of oxygen bubbles through the catalyst layer or porous transport layer [23].

Similarly to the increase in performance at high currents from the IV curve analysis, the decrease in HFR can be connected to a decrease in ohmic resistance of the membrane (enhanced conductivity and thinning), and improved contacts among the different components of the cell [24]. The observed decrease in HFR is 15.4mΩcm$^2$ over the whole duration of the test would lead to a thinning-induced voltage decrease rate of −61 μV h$^{-1}$at 2.0Acm$^{-2}$, but the observed rate lies at −25 μV h$^{-1}$. Therefore, it can be inferred that different mechanisms occur simultaneously. The previously reported mechanisms that affect cell potential are membrane thinning [25], structural adjustments of the CL [9], improvement of ionic conductive pathways [11], catalyst degradation/loss [11], and Ti-PTL passivation [9]. The total ohmic resistance of all cells increases, with experiment $cyc_{10s}$ and *solar*being the exceptions, where a decrease was observed. Fig. 9 shows the evolution of the HFR normalized by the initial values for all operation modes.

The HFR when cycling at 100 s dwell time ($cyc_{100s}$) increases slightly by around 4% during the first period and stays constant for the rest of the test. On the other hand the HFR increases continuously for constant current operation (experiment *cc*) over the entire test period, reaching around 25% increase after 500 h. This behavior has been observed in the literature [8], where constant operation at 2Acm$^{-2}$ as well as cycling with a 6-h period show a similar trend. An increase in HFR has previously been reported and connected to impurities within the membrane and Ti-PTL passivation [9,12]. It is

Please cite this article as: Frensch SH et al., Influence of the operation mode on PEM water electrolysis degradation, International Journal of Hydrogen Energy, https://doi.org/10.1016/j.ijhydene.2019.09.169

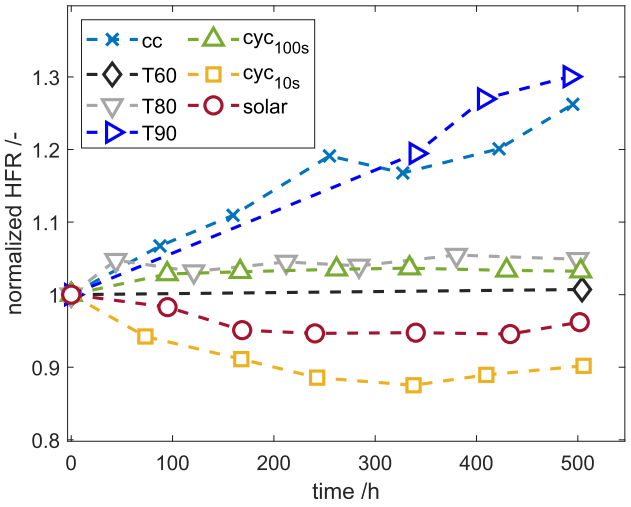


**Fig. 9 – Comparison of HFR relative to the beginning of life for all experiments over time.**

reported that a thin oxide layer builds up on the Ti-PTL, which increases the ohmic resistance.

The faster dynamic operation modes, experiments $cyc_{10s}$ and *solar*exhibit an increase in performance over the first approximately 300 h, mostly associated to a decrease in ohmic resistance, while all other experiments behave the opposite. However, since these dynamic operation modes are similar to the applied break-in procedure, the improvement seen could be an extension of the break-in process, where beneficial structural changes within the layers and removal of impurities continue to happen.

Meanwhile, low-frequency cycling may not have a positive impact due to the long periods at constant potential. The time between a potential change in experiments $cyc_{10s}$, *solar*, and $cyc_{100s}$ are 10 s, 60 s, and 100 s, respectively. Therefore, the threshold dwell time above which no positive effect is observed anymore lies between 60 s and 100 s. Furthermore, a possible explanation may be that the bubble growth under a constant signal leads to a resistance increase [23,26]. In this case, the bubbles are suspected to further locally dehydrate the membrane. When a shift in potential occurs, the bubbles may experience a faster detachment or change in growth behavior, which is beneficial for membrane hydration and therefore durability. It has been reported that low-frequency cycling (0–2.0Acm$^{-2}$, 6 h each) led to a decrease in HFR, compared to an increase for constant operation at 2.0Acm$^{-2}$, whereas a 10-min cycle showed a more or less constant HFR after 500 h [8]. However, they did not observe a voltage decrease in any of their operation modes, which were constant current or had more than 100 s dwell time. A stack operated at up to 4.0Acm$^{-2}$ under different operation modes showed a decrease in HFR and potential, and exhibited fluoride emission while no membrane thinning was observed [11]. The authors connected the decrease in HFR to improved ionic conductive pathways, and the increase in overall cell performance over time to the fact that positive phenomena dominate over the negative ones, such as Ti-passivation.

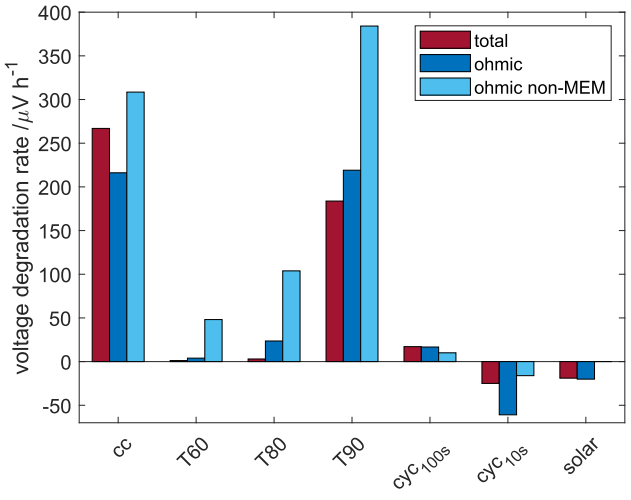


**Fig. 10 – Separation of the impact of processes on the voltage degradation rates at 2.0Acm$^{-2}$. The total is extracted from IV curves, ohmic from the change in HFR, and ohmic non-membrane (MEM) is the membrane-thinning-corrected value extracted from the HFR.**

### *Separation of degradation mechanisms*

In the following, it is attempted to separate the total ohmic change into its components, membrane thinning and PTL. The PTL contribution consists of Ti passivation and the suspected positive effect of MEA adjustments to the PTL, which may however also have an impact on the non-ohmic overpotential. Ti passivation has in fact been reported in connection with the ohmic resistance [8,18] as well as in connection with the high frequency arc in the Nyquist plot [11]. This work attempts to identify the purely ohmic contribution and therefore investigates the effect on HFR.

A thinning of the membrane over time results in a decrease of its overpotential due to the linear relationship according to Ohm's law. The theoretical decrease in cell voltage due to this thinning is calculated and subtracted from the total voltage degradation rate due to ohmic phenomena measured from the HFR at 2.0Acm$^{-2}$. A constant membrane conductivity of 15S m$^{-1}$, which is seen as the upper limit, is assumed for this analysis [22,27]. The result is a voltage degradation rate due to all other ohmic phenomena than membrane thinning and is shown in Fig. 10. For comparison, the total cell voltage degradation rate as measured from the IV curves as well as the voltage degradation rate extracted from the change in HFR are also shown.

It can be seen that the membrane-thinning-corrected value is highly affected by the temperature, as it increases from 104 μV h$^{-1}$at 80 °C to 384 μV h$^{-1}$at 90 °C. A reasonable explanation is the previously suggested passivation of the Ti-PTL, which increases the contact resistances of the anode PTL. Ti-passivation has been observed in the literature [9,10] and is enhanced at elevated temperatures [28]. The value is reduced to 10 μV h$^{-1}$when cycling at 100 s dwell time ($cyc_{100s}$), where the lower extent of titanium passivation may be explained by a lower residual time of oxygen within the electrode for cycling operation, which was earlier suggested as a reason for lower local membrane dehydration. The negative value for $cyc_{10s}$ suggests that a beneficial ohmic phenomenon, possibly

Please cite this article as: Frensch SH et al., Influence of the operation mode on PEM water electrolysis degradation, International Journal of Hydrogen Energy, https://doi.org/10.1016/j.ijhydene.2019.09.169

due to improved contact between MEA and PTL, is dominant over PTL passivation.

Experiments $cyc_{10s}$ and *solar*show a decrease in HFR along with a high fluoride emission rate. However, membrane thinning was not found to be more severe compared to the other operation modes. This points to the cathode CL binder as a source of the fluoride rather than the membrane. This fluoride loss seems to improve the structure and therefore performance of the CL as the cell voltage decreases over time. The changing point is after around 300 h, where the HFR starts to slowly increase, perhaps due to dominant PTL passivation or other processes such as irreversible cation contamination.

## Conclusion

An analysis of degradation phenomena in PEM WE with a focus on the impact of different operation modes was presented. Therefore, seven MEAs with the same specifications were tested for 500 h each at the different operation modes, which included varying operating temperatures and different current cycling modes. It was found that the anode catalyst layer only played a minor role on degradation, while a change in total ohmic resistance dominated the voltage change. Subsequently, the respective shares of membrane and porous transport layer related phenomena were quantified.

Operation at 90 °C is favorable in terms of efficiency, but was found to significantly increase the fluoride emission rates and membrane thinning over time. Therefore, higher temperature can limit the lifetime considerably due to increased gas crossover for a thinner membrane, while Ti passivation may counter the gain in efficiency over time without an appropriate mitigation strategy.

Finally, fast cycling operation modes, inluding the simulated solar PV profile increased the overall performance over the investigated time frame due to a decrease in ohmic resistance. It was also found that fluoride emission is enhanced with fast potential switches, with no significant impact on the membrane thickness, which may imply that most of the fluoride emission originates from the cathode catalyst layer.

## Acknowledgement

The authors would like to acknowledge the support by Innovation Fund Denmark through the e-STORE project, Grant 4106-00025B.

## REFERENCES

[1] Arico AS, Siracusano S, Briguglio N, Baglio V, Di Blasi A, Antonucci V. Polymer electrolyte membrane water electrolysis: status of technologies and potential applications in combination with renewable power sources. J Appl Electrochem 2013;43(2):107–18. https://doi.org/10.1007/s10800-012-0490-5.

[2] Borah D, Carmo M, Müller M, Lehnert W. Modelling and simulation activities on PEM water electrolysis. 2017. p. 52425.

[3] Bensmann B, Hanke-Rauschenbach R, Müller-Syring G, Henel M, Sundmacher K. Optimal configuration and pressure levels of electrolyzer plants in context of power-to-gas applications. Appl Energy 2016;167:107–24. https://doi.org/10.1016/j.apenergy.2016.01.038.

[4] Olah GA, Goeppert A, Prakash GS. Beyond oil and gas: the methanol economy. Wiley-VCH; 2009.

[5] Godula-Jopek A. Hydrogen production by electrolysis. Wiley-VCH; 2015.

[6] Oi T, Sakaki Y. Optimum hydrogen generation capacity and current density of the PEM-type water electrolyzer operated only during the off-peak period of electricity demand. J Power Sources 2004;129(2):229–37. https://doi.org/10.1016/j.jpowsour.2003.11.050.

[7] Bessarabov D, Wang H, Li H, Zhao N. PEM electrolysis for hydrogen production –– principles and applications. CRC Press; 2016.

[8] Rakousky C, Reimer U, Wippermann K, Kuhri S, Carmo M, Lueke W, Stolten D. Polymer electrolyte membrane water electrolysis: restraining degradation in the presence of fluctuating power. J Power Sources 2017;342:38–47. https://doi.org/10.1016/j.jpowsour.2016.11.118.

[9] Rakousky C, Reimer U, Wippermann K, Carmo M, Lueke W, Stolten D. An analysis of degradation phenomena in polymer electrolyte membrane water electrolysis. J Power Sources 2016;326:120–8. https://doi.org/10.1016/j.jpowsour.2016.06.082.

[10] Fouda-Onana F, Chandesris M, Médeau V, Chelghoum S, Thoby D, Guillet N. Investigation on the degradation of MEAs for PEM water electrolysers part I: effects of testing conditions on MEA performances and membrane properties. Int J Hydrogen Energy 2016;41:16627–36. https://doi.org/10.1016/j.ijhydene.2016.07.125.

[11] Lettenmeier P, Wang R, Abouatallah R, Helmly S, Morawietz T, Hiesgen R, Kolb S, Burggraf F, Kallo J, Gago AS, Friedrich KA. Durable membrane electrode assemblies for proton exchange membrane electrolyzer systems operating at high current densities. Electrochim Acta 2016;210:502–11. https://doi.org/10.1016/j.electacta.2016.04.164.

[12] Sun S, Shao Z, Yu H, Li G, Yi B. Investigations on degradation of the long-term proton exchange membrane water electrolysis stack. J Power Sources 2014;267:515–20. https://doi.org/10.1016/j.jpowsour.2014.05.117.

[13] Inaba M, Kinumoto T, Kiriake M, Umebayashi R, Tasaka A, Ogumi Z. Gas crossover and membrane degradation in polymer electrolyte fuel cells. Electrochim Acta 2006;51(26):5746–53. https://doi.org/10.1016/j.electacta.2006.03.008.

[14] Liu W, Ruth K, Rusch G. Membrane durability in PEM fuel cells. J New Mater Electrochem Syst 2001;4(4):227–32. https://doi.org/10.1002/fuce.200320239.

[15] LaConti AB, Liu H, Mittelsteadt C, Giner RCM. Polymer electrolyte membrane degradation mechanisms IN fuel cells – findings over the past 30 years and comparison with electrolyzers. ECS Transactions 2006;1(8):199–219.

[16] FCH-JU. ANNUAL WORK PLAN and BUDGET. Tech. rep. FCH-JU; 2017.

[17] Cherevko S. Stability and dissolution of electrocatalysts : building the bridge between model and " real world " systems. Curr Opin Electrochem 2018:1–8. https://doi.org/10.1016/j.coelec.2018.03.034.

[18] Siracusano S, Hodnik N, Jovanovic P, Ruiz-Zepeda F, Šala M, Baglio V, Aricò AS. New insights into the stability of a high performance nanostructured catalyst for sustainable water

electrolysis. Nano Energy 2017;40(September):618–32. https://doi.org/10.1016/j.nanoen.2017.09.014.
[19] Ruvinskiy PS, Bonnefont A, Pham-Huu C, Savinova ER. Using ordered carbon nanomaterials for shedding light on the mechanism of the cathodic oxygen reduction reaction. Langmuir 2011;27(14):9018–27. https://doi.org/10.1021/la2006343.
[20] Chandesris M, Médeau V, Guillet N, Chelghoum S, Thoby D, Fouda-Onana F. Membrane degradation in PEM water electrolyzer: numerical modeling and experimental evidence of the influence of temperature and current density. Int J Hydrogen Energy 2015;40(3):1353–66. https://doi.org/10.1016/j.ijhydene.2014.11.111.
[21] Büchi FNF, Inaba M, Schmidt TJTTJ. Polymer electrolyte fuel cell durability. Springer; 2009.
[22] Ito H, Maeda T, Nakano A, Takenaka H. Properties of Nafion membranes under PEM water electrolysis conditions. Int J Hydrogen Energy 2011;36(17):10527–40. https://doi.org/10.1016/j.ijhydene.2011.05.127.
[23] Lee C, Banerjee R, Arbabi F, Hinebaugh J, Bazylak A. Porous transport layer related mass transport losses in polymer electrolyte membrane electrolysis –– a review. In: Proceedings of the 14th international conference on nanochannels, microchannels, and minichannels; 2016.
[24] Niya SMR, Phillips RK, Hoorfar M. Process modeling of the impedance characteristics of proton exchange membrane fuel cells. Electrochim Acta 2016;191(May):1–117. https://doi.org/10.1016/j.electacta.2016.01.128.
[25] Siracusano S, Van Dijk N, Backhouse R, Merlo L, Baglio V, Arico A. Degradation issues of PEM electrolysis MEAs. Renew Energy 2018;123:52–7. https://doi.org/10.1016/j.renene.2018.02.024. http://linkinghub.elsevier.com/retrieve/pii/S0960148118301678.
[26] Kiuchi D, Matsushima H, Fukunaka Y, Kuribayashi K. Ohmic resistance measurement of bubble froth layer in water electrolysis under microgravity. J Electrochem Soc 2006;153(8):E138. https://doi.org/10.1149/1.2207008. http://jes.ecsdl.org/cgi/doi/10.1149/1.2207008.
[27] Kusoglu A, Kienitz BL, Weber AZ. Understanding the effects of compression and constraints on water uptake of fuel-cell membranes. J Electrochem Soc 2011;158(12):1504–14. https://doi.org/10.1149/2.097112jes.
[28] Lu G, Bernasek SL, Schwartz J. Oxidation of a polycrystalline titanium surface by oxygen and water. Surf Sci 2000;458(1):80–90. https://doi.org/10.1016/S0039-6028(00)00420-9.

Please cite this article as: Frensch SH et al., Influence of the operation mode on PEM water electrolysis degradation, International Journal of Hydrogen Energy, https://doi.org/10.1016/j.ijhydene.2019.09.169